In-water Electrical Impedance Tomography: EIT and the Sea

Andy Adler[1], Tarek el Harake[1], Martina Mosing[2], Andreas Fahlman[3]
[1]Carleton University, Ottawa, Canada
[2]Department for Small Animals and Horses, Veterinary University Vienna , Vienna, Austria
[3]Global Diving Research SL, Sanlucar de Barrameda, Spain

Corresponding Author: andy.adler@carleton.ca

Abstract

Objective: Electrical impedance tomography (EIT) has shown the ability to provide clinically useful functional information on ventilation in humans and other land mammals. We are motivated to use EIT with sea mammals and human divers, since EIT could provide unique information on lung ventilation that can help address diver performance and safety, and veterinary and behavioural questions. However, in-water use of EIT is challenging, primarily because sea water is more conductive than the body. *Approach:* We first address this issue by modelling the in-water component and evaluating image reconstruction algorithms. *Main Results:* EIT is able to produce reasonable images if an outer insulating layer allows a water layer thickness < 2% of the body radius. We next describe the design of custom EIT belts with an outer neoprene insulator to minimize current leakage. We show example underwater EIT recordings in human and dolphin subjects. *Significance:* we demonstrate in-water EIT is feasible with appropriate techniques.

Funding Acknowledgement

ONR award #: N000142312002

Introduction

Diving mammals seek to maximize time underwater but must eventually surface to exchange metabolic gasses. Human breath-hold divers face similar challenges, while SCUBA divers are constrained by the limitations of their breathing apparatus. Breathing in aquatic mammals is poorly understood; of particular interest are changes in the respiratory mechanics while diving (Lemaitre et al 2009; Fahlman, 2024). During diving, increasing pressure causes alveolar compression and a depth-dependent pulmonary shunt that eventually results in alveolar collapse and cessation of gas exchange (Fahlman et al., 2021a). A better understanding of the gas distribution of the lungs and resulting changes in gas exchange with depth could lead to novel clinical management and perhaps explain stress-associated stranding of marine mammals (Fahlman et al 2021a).

To study respiratory mechanics in freely swimming subjects, e.g. marine mammals and humans, improved instrumentation to measure respiratory and cardiovascular function in water is necessary. In diving mammals, such instrumentation would help elucidate the respiratory and cardiovascular adaptations to diving, including how exercise- and breathing-physiology factors affect diving capacity (Fahlman et al 2020). In human divers on SCUBA or using rebreathers, we want to understand the effect of training, postures, manoeuvres and fatigue on performance and physiology.

Unfortunately, instrumentation for in-water physiological measurements is limited. Currently, the most common instruments for divers use inertial measurements (accelerometers and gyros) and pressure measurements for depth (Fahlman et al., 2021b). These are useful to evaluate diving behaviour and can be used as proxies for diving capacity, but do not measure physiological processes. Breathing measurements (upon surfacing) have been made with spirometers, either in a diver's mask or held onto a blowhole (Fahlman, 2024). Spirometers provide high-quality breathing data, but cannot collect measurements in freely moving subjects. Cardiovascular measurements have been made using body surface ECG and pulse oximetry (Fahlman et al., 2021b). Unfortunately, both measurements are very sensitive to movement artefacts and require extensive data cleaning in active subjects.

Electrical Impedance Tomography (EIT) could potentially provide a valuable contribution. EIT can measure gas flow within the airways, allow an estimate of tidal volume and functional residual capacity as well as the redistribution of lung gasses as a function of hydrostatic pressure; it is also sensitive to the movement of conductive blood and can provide information on perfusion and cardiac output (Frerichs et al, 2017, Brabant et al, 2022). EIT offers several potentially compelling advantages either as a stand-alone instrument or in conjunction with other physio-logging devices.

The key challenge to in-water bioimpedance measurements is that the conductivity, σ, of sea water is much larger than that of tissue. Seawater has a mean $\sigma = 6$ S/m at the surface, and this value decreases with depth and varies by 20% in different oceans depending on salt content (Zheng et al 2018). The most conductive tissues, such as blood, have an order of magnitude lower conductivity, $\sigma \leq 0.7$ S/m. Given this difference, current from body-surface electrodes will preferentially flow in the water, rather than the body. Initial experiments (Adler et al 2021) showed a dramatic reduction in signal strength due to the seawater; regular EIT electrodes placed on the body leave very small signals corresponding to body physiology. These signals are very sensitive to movements of the body, and gathering useful data was impossible. However, when covering the body in an insulating neoprene layer useful data were gathered (Adler et al 2024). Such a layer reduces the thickness of the seawater layer, and leads to improved EIT signals.

The aim of this study was to quantify and then address challenges to in-water EIT, and to demonstrate the feasibility of such measurements in dolphins and humans. Our paper is organized as follows: first, we investigate numerically the effect of sea water on the EIT signal and reconstruction images. Next, we describe the development of electrode belts

suitable for in-water EIT measurements. Finally, we demonstrate the feasibility of EIT during spontaneous breathing while submerged in sea water in the dolphin and human.

Methods: Numerical

The first step was to understand the current flow in the water near an electrode covered with an insulating cap. We explored this phenomenon in figure 1, using a finite element model (FEM) to simulate a body with current flowing between two electrodes covered by a non-conducting snap. The current density when surrounded by air (1A) shows the normal pattern, high current density at the electrode margins. When surrounded by conductive fluid, most current flows in the fluid (1C–1F). Even when the snap is very close to the body (1F), current prefers flowing in fluid after it has passed the cap boundary.

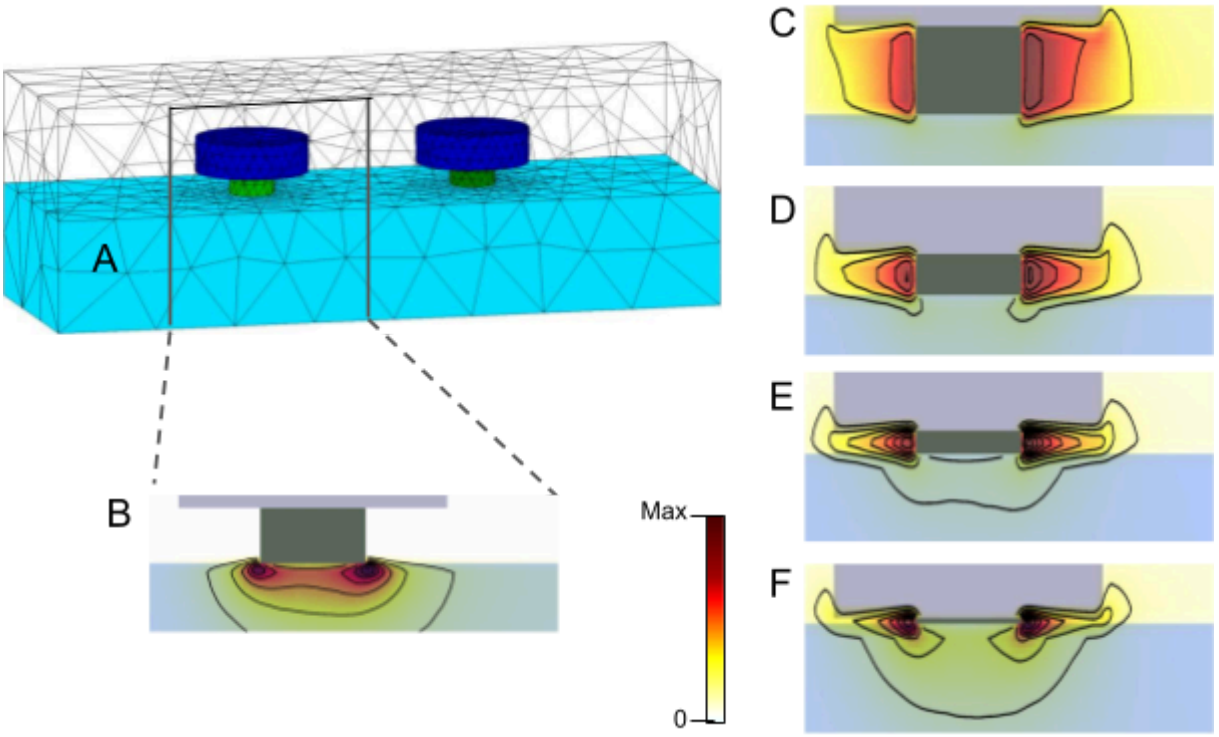

Figure 1: Current flow between two body-surface electrodes in a model in air and saltwater. A) FEM of a body (light blue) with two electrodes (green) covered by a non-conductive snap (dark blue). B–F) Current density in a central slice of the FEM, shown with respect to the colourbar and contour levels as iso-current lines. B) Current into the body when the outside is non-conductive air. Images C, D, E and F show current in seawater with conductivity 5× the body. The thickness of the exposed electrode varies from 0.2 (C), 0.1 (D), 0.05 (E), 0.02 (F)

Based on the first FEM simulation, illustrating that covering each single electrode will not force the current to flow into the body, a second model was calculated where a medium (body) with surface electrodes is surrounded by another medium of variable thickness (seawater layer between body and layer of insulating belt material):

In order to quantify the changes in EIT signals due to a surrounding conductive medium, we use the FEM model of figure 2. Here, a cylindrical medium of radius 1.0 and height 2.0 has 16 electrodes placed at half the height. The medium is surrounded by another region of thickness t_W. The FEM is created in EIDORS (Adler and Lionheart, 2006), and internal electrodes are created by meshing internal cylindrical regions, and then hollowing the region and replacing the surface with the complete electrode model (Cheng et al 1989). FEM elements are refined in Netgen (Schöberl 1997) in the central region by specifying a maximum element size of 0.01 in a cloud of points at the electrode plane. Cylindrical target regions are created with various radii, r_t, centred on the electrode plane with half the tank height.

Using this FEM, EIT signals are simulated, assuming a body conductivity of 1.0 and a seawater conductivity of σ_W in a region of thickness t_W, representing the water under an insulating layer covering the body. A current of 1.0 mA is applied across pairs of electrodes and the voltages on all other electrode pairs measured, except for electrodes which are part of the driven pair. Electrode pairs are defined on the basis of a *skip* pattern, S, so electrode k is paired with electrode (k+S mod 16). The adjacent stimulation and measurement pattern corresponds to S=0, while S=8 indicates the opposite pattern. The vector of voltages, $\mathbf{v}_h(t_W, \sigma_W, S)$, represents a frame of EIT data for measurements across all pairs for the indicated water thickness and conductivity and skip, S. Similarly, $\mathbf{v}_t(t_W, \sigma_W, S)$ represents the frame of measurements with a conductivity-contrasting target.

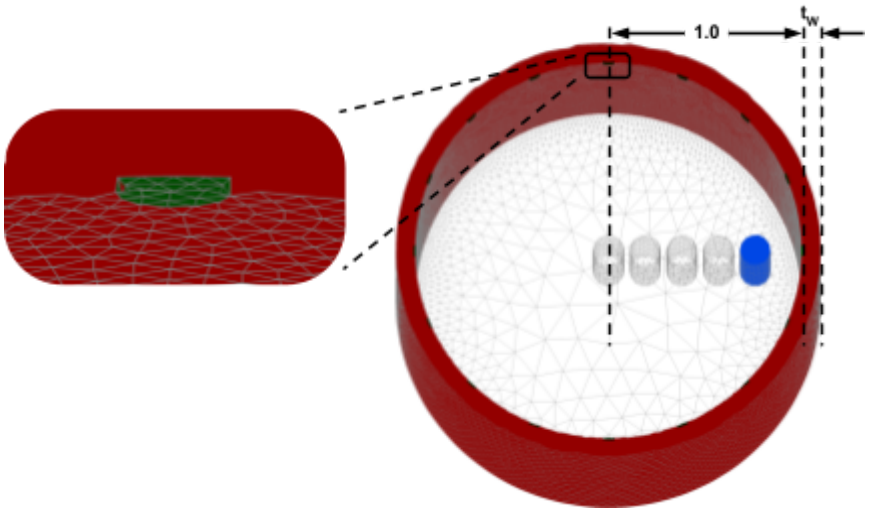

Figure 2: Finite element model used, sliced at the electrode plane. Right: a cylindrical body is simulated with radius=1.0 and surrounded by 16 electrodes (green) and a conductive seawater layer of thickness t_w. Left: Inset of hollow electrode (green). Cylindrical targets are placed at radial distances from the centre.

Using the FEM of Figure 2, we simulate the loss of signal associated with the surrounding seawater as a function of its conductivity, σ_W, and layer thickness t_W. The signal is defined as the norm, $\| (\mathbf{v}_t - \mathbf{v}_h) ./ \mathbf{v}_h \| = \| \mathbf{v}_t ./ \mathbf{v}_h - 1 \|$, where "./" is the Hadamard (element-by-element) division operation. Figure 3 shows the signal as a function of σ_W and t_W, for a signal at the medium centre. The scenario σ_W=0 corresponds to a medium surrounded by air and thus has a constant signal independent of t_W. On the other hand the signal decreases rapidly at large t_W,

with an asymptote at approximately $1/\sigma_W$, such that seawater with 20× the body conductivity has a little less than 5% of the EIT signal. The EIT signal strength is also a function of the radial position (figure 2, right). Target positions closer to the boundary have slightly less signal loss than those in the centre, for the same water conductivity.

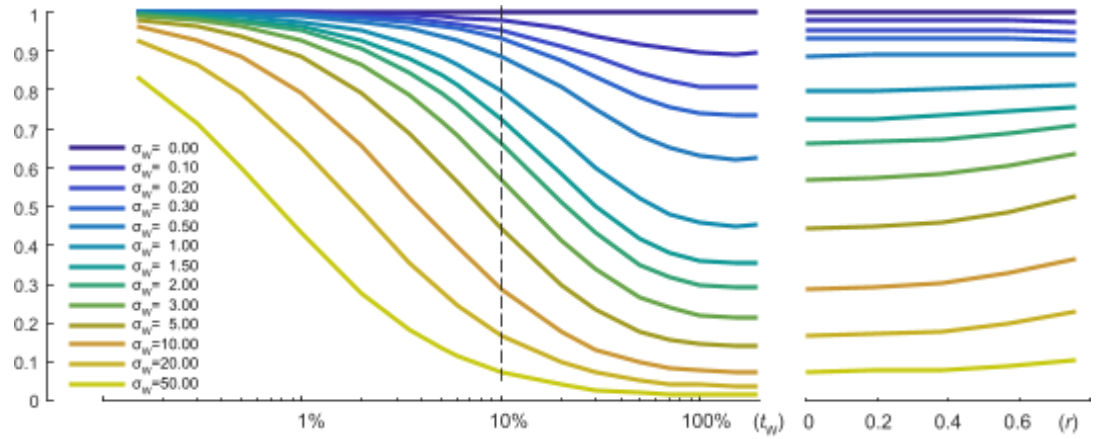

Figure 3: Difference signal, $||\mathbf{v}_t./\mathbf{v}_h - 1||$ with skip S=0, as a function of (left) water-layer conductivity (σ_W vs medium conductivity, σ=1) and thickness (t_W), for a target placed at the centre; and (right) as a function of target radial position (for t_W=10%, corresponding to the dotted line). Signals are normalized with respect to an air (σ_W=0) outer layer.

In order to understand the effect of the seawater layer of σ_W=10 on the reconstructed signals, we show reconstructed images in Figure 4. Using a GREIT algorithm (Adler et al 2009) which assumes no conductive outer layer, EIT images of a target at radial position r=0.75 are shown for various values of skip and t_W. While for regular (in-air) EIT, the image maximum is aligned with the correct radial position, conductive surroundings "push" the image toward the centre, and this effect increases with t_W, in a way that is roughly independent of skip. However, the overall shape distortion is worse with low skip values. Additionally, the presence of a seawater layer dramatically reduces the image amplitude. Each EIT image contour is normalized to its own maximum; for S=2, the EIT images amplitude (Σ image pixels) is reduced to 84%, 33% and 5% of its value at t_W=0% for t_W= 2%, 10%, 50%.

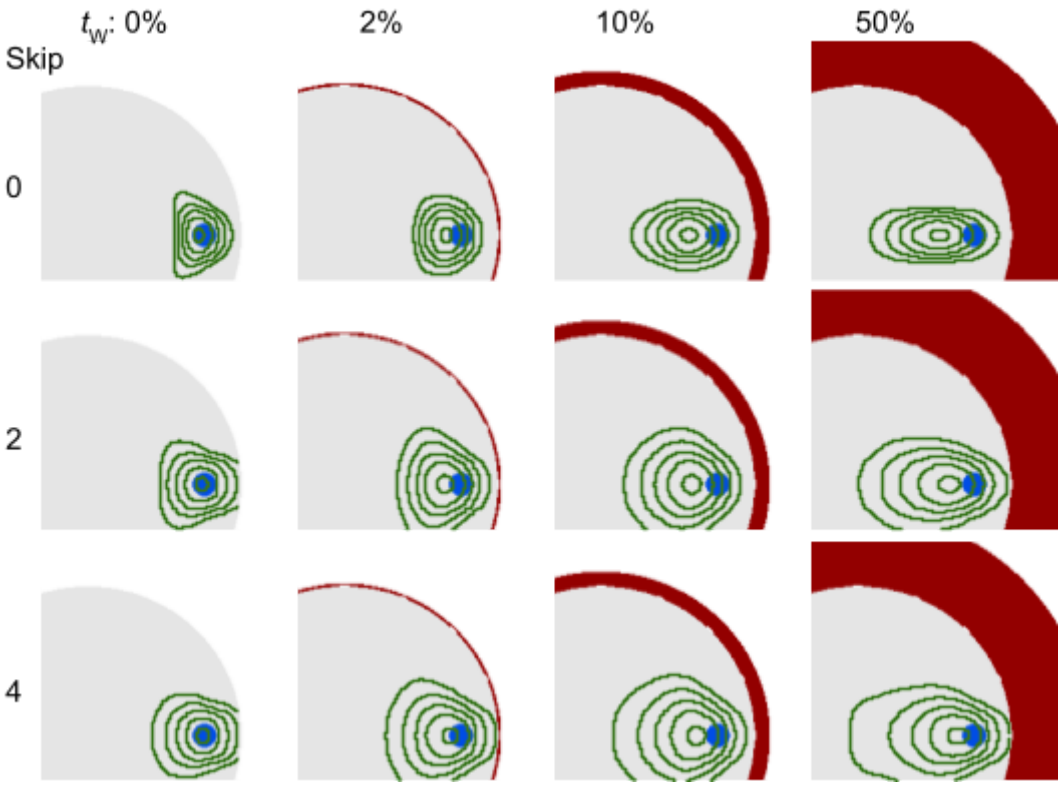

Figure 4: Reconstructions as a function of skip pattern (0,2,4 from left to right) and the thickness of the conductive water layer (σ_W=10), shown in red (t_W, as a % increase in medium radius, where 0% indicates no water layer). A small cylindrical target (blue cylinder) is simulated, and the contour lines show the reconstructed image as a fraction of maximum (20%,40%,60%,80%,95%).

We interpret our numerical results as follows. If t_W = 2% and $\sigma_W/\sigma < 20$ then the signal strength (figure 3) is above 50%, the image amplitude is ~85% and the image distortion is relatively small (figure 4). We thus set $t_W < 2\%$ as our design goal for the next section.

Methods: Hardware and Validation

Based on our numerical results, we require an EIT belt system with an electrically insulating layer which ensures there is only a thin layer of seawater next to the body. For a human diver, the minimum chest radius is 10 cm, and 2% of the radius corresponds to 2 mm of water between the body and an insulating layer. This is feasible with a tight neoprene belt. In our human experiments, we estimated the water-layer thickness by palpating the neoprene on the subject. Since dolphins were free swimming, we assured that the belt was placed as tightly as we could while prioritizing subject comfort. We therefore estimate, but are not certain, that we achieve t_w<2%.

Figure 5 shows our EIT belt and insulating layer system. Electrodes are made with a conductive carbon film (Haouger Electronic Technology, Shanghai). We evaluated six different conductive electrode materials, and selected this one based on its performance in preliminary tests. At the back of each electrode, an ECG-type snap is attached. EIT cables attach to the snaps and then to a Sentec pioneer set (Landquart, Switzerland) for data

acquisition. All Data were collected at 47.7 frames / s. The maximum length of each cable is 3 m. An outer neoprene layer contains the cables, electrodes, and connectors to minimize current leakage. Neoprene has very low conductivity and is used as an electrical insulator. All parts attach with velcro. Several sizes of belts were made for human and dolphin subjects. To minimize water next to the skin, belts were attached tightly to each subject.

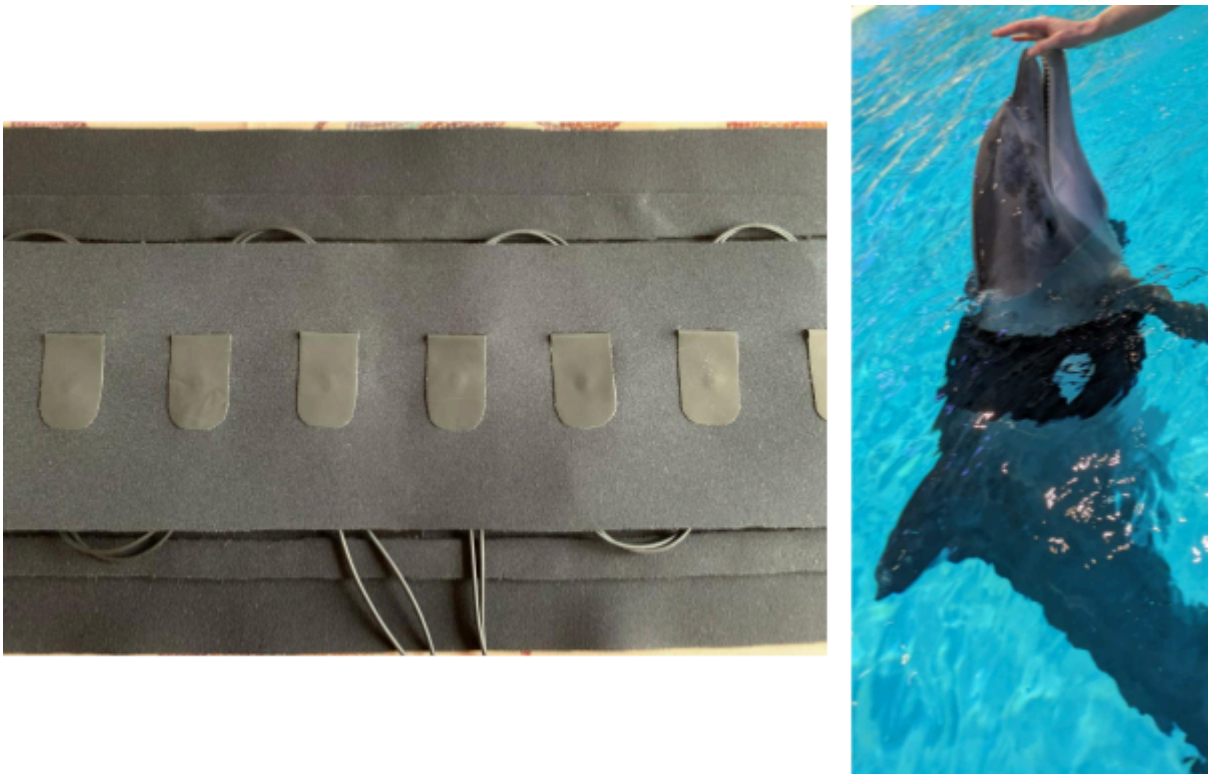

Figure 5: Modified EIT belt and its use on a dolphin. Left: The EIT electrodes are made of conductive carbon film with a rear snap connector to the cables. All other parts are neoprene, including an outer layer to prevent current leakage. Right: The belt placed on a dolphin during habituation.

Tests in human subjects: Tests in human participants were performed with informed consent, in accordance with the principles embodied in the Declaration of Helsinki and in accordance with local statutory requirements (Carleton university research ethics #119709). For human subjects we used two belts of 16 electrodes (twice the belt shown in figure 5) configured for 3D EIT with a square-pattern electrode layout (Grychtol et al 2019). The EIT data acquisition was configured to use skip 4, which roughly corresponds geometrically to skip 2 for 16 electrodes.

The 55-year old, 76 kg adult male subject lay in a 4 m×1 m×1 m water tank into which salt was added to approximate seawater. The subject lay supine on the tank bottom and breathed through a snorkel-type tube. The subject was instructed to perform tidal breathing, followed by a maximal inspiration and expiration each held for between 6-7s, i.e. brief inspiratory and expiratory breath hold, followed by tidal breathing.

EIT data were filtered with a notch filter to remove 9.32–9.48 Hz (to compensate for aliasing in the Sentec Pioneer set) and a 3rd order Butterworth low-pass filter at 30 Hz. Images were reconstructed with 3D GREIT (Grychtol et al 2019) onto a 32×32×9 grid using a human adult male FEM geometry with a noise figure of 0.3.

Tests in dolphins: Tests in dolphins were performed under animal care approval from Oceanografic Valencia (IACUC: OCE-18-21-22 and also BUMED: NRD#1286). The subject was a 77 kg male rough toothed dolphin (*Steno bredanensis*), that had been found stranded and brought into a rehabilitation facility and deemed unreleasable (and thus of unknown age). This dolphin was diagnosed with persistent pneumonia. Experiments were conducted using operant conditioning: before the start of the study animals were desensitized to the equipment and trained for the specific research-associated behaviors. The dolphin was not restrained and could withdraw from the research trial at any time.

Measurements were done at the poolside at an aquarium. The belt with 16 electrodes was placed onto the dolphin which held its body calmly for a 4-minute data recording. During this time, the dolphin performed 13 spontaneous breaths. In addition to EIT measurements, the dolphin breathed through a custom built pneumotachometer (CetaSpiro, G&O embedded systems, Switzerland). Flow data were corrected to Standard Temperature Pressure Dry (STPD), integrated to estimate tidal volume, and scaled to match the global EIT waveform.

EIT data were filtered with a 3rd order low-pass filter at 5 Hz. The belt used an interleaved connection by which the 32 electrode channels of the Sentec Pioneer set were each connected to two electrodes in the 16 electrode belt, in a way which provided both skip 4 and skip 0 data. In post-processing, it was decided that the skip 0 fraction of the data gave better image resolution, and only the skip 0 results were used. Images reconstructed with 2D GREIT (Adler et al 2009) with noise figure 0.3 onto a 32×32 grid using an elliptical cylinder geometry with eccentricity 0.33. Data and software used in this paper are available at doi.org/10.5281/zenodo.14779620

Results

Human: Using our developed belt and the collected human data, images were reconstructed with the 3D GREIT algorithm and the images at the upper and lower electrode planes shown. Figure 6 shows a sample of the recorded results during tidal breathing while the subject was supine and 50 cm below water. A waveform region is selected during which maximum breaths and inspiratory hold correspond to a dolphin's breath. The EIT reference is also chosen at end inspiration (14–16 s) so that loss of air during expiration is shown. The figure shows that lung regions are temporally synchronized. Typically, flow in lung regions shows some variability even in healthy patients. In this case, at a more uniform global pressure (~50 cmH_2O), the lung may be showing increased regional uniformity. Figure 6 also shows the effect of an electrode disconnection (at t=21 s). At this point, during a forced exhale, the chest moves in a way that a left-ventral electrode disconnects.

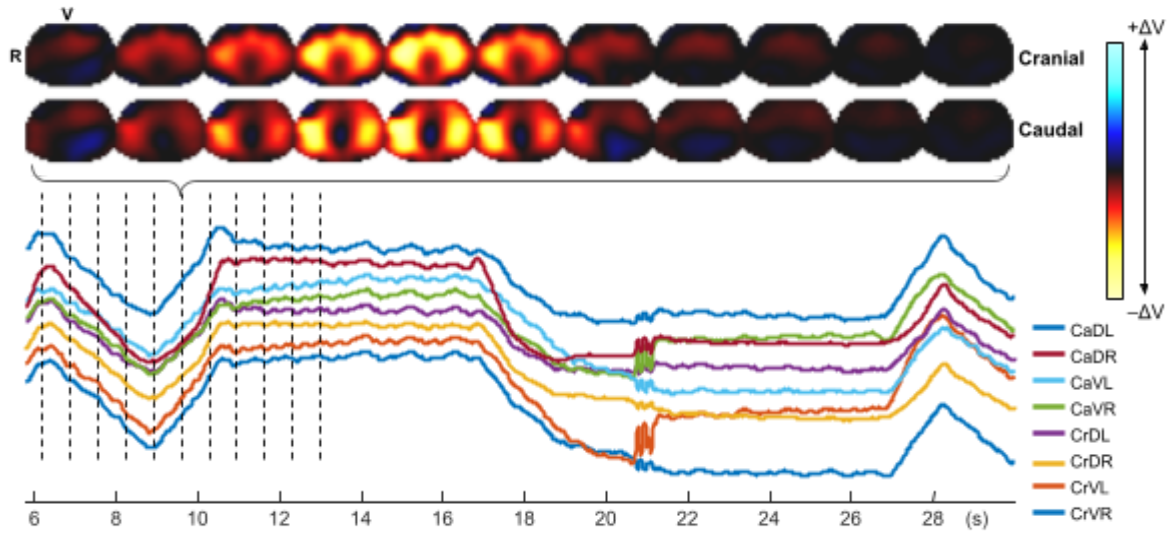

Figure 6: EIT results from an in-water healthy human volunteer. Top row, transverse EIT images at the Cranial and Caudal EIT belt positions (with orientation (V)entral and (R)ight as shown). Right: colour mapping for increases and decreases in air volume. Images correspond to the dotted lines in the EIT waveforms below. Regions of interest are shown for (Cr)anial/(Ca)udal, (V)entral/(D)orsal, and (R)ight/(L)eft. Note the electrode disconnect artefact at *t*=21 s. The breath between *t*=10 s and *t*=27 s represents an inspiratory breath hold for 7 seconds, followed by an expiratory breath hold for 6 seconds.

Dolphin EIT results were reconstructed from a single plane of 16 electrodes using the skip 0 data. Figure 7 shows a portion of the data in which the dolphin took two spontaneous breaths. The global EIT signal (black) corresponds closely in timing and amplitude to the integrated spirometer signal (dark blue). Transverse EIT images are rotated to show the anatomical position of the dolphin, and show air moving first from the ventral part of the lung, and then from the central regions. This regional delay can also be seen in the horizontal-ROI EIT waveforms. There is a clear delay between the ventral and central waveforms starting at 222.2 s. This delay may be due to the persistent pneumonia in this animal. The dolphin was close to the surface during the collection of these data, and the lung pressure was on average ~20 cmH_2O.

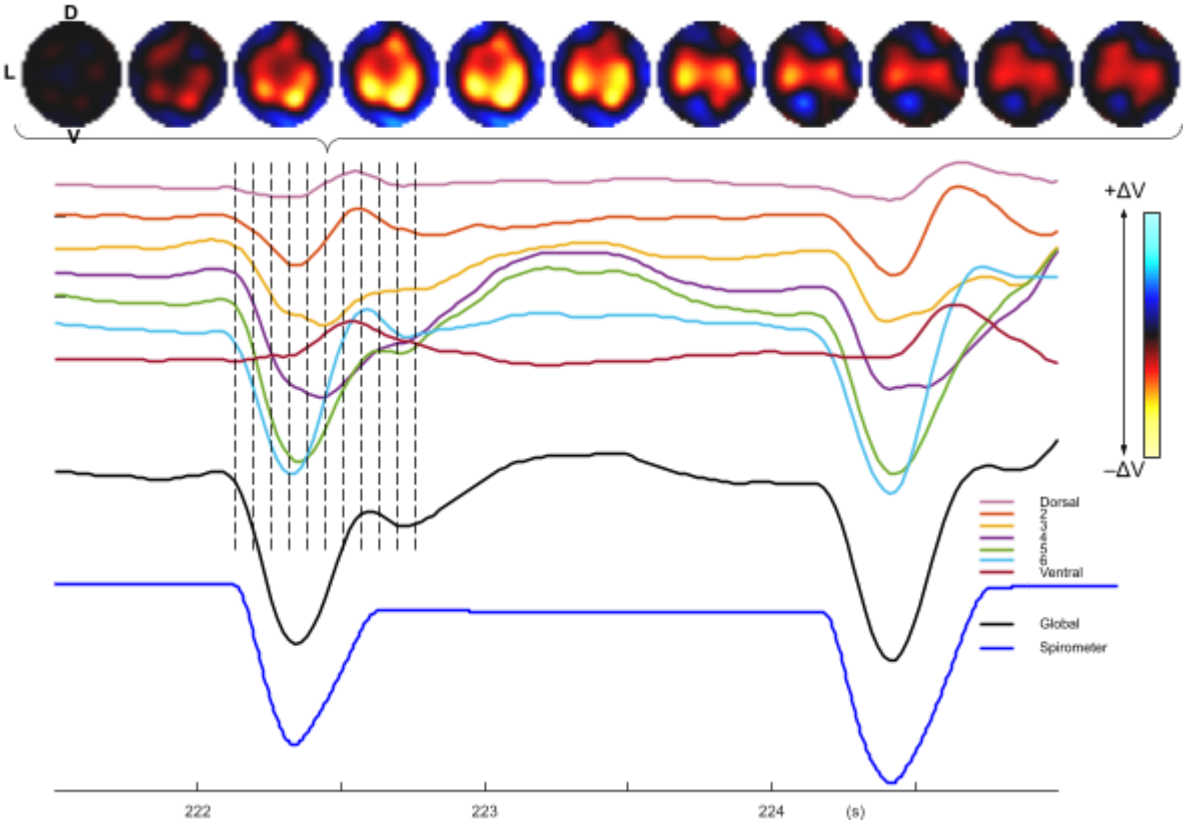

Figure 7: EIT results from an in-water dolphin with suspected bronchitis (Dorsal, D, Left, L, and Ventral V, indicated). Time (bottom) is seconds since the start of recording. Two breaths (exhale then inhale) are shown. EIT waveforms correspond to regions of interest from the Dorsal (top) to Ventral (bottom) of the thorax cross section. The Global EIT waveform is shown in black, and spirometer volume in blue. Lung volume corresponds to an increase in waveform. EIT images (bottom) correspond in time to the dotted lines. The EIT reference is the average during $221.5 < t < 222$ s. Note the initial air exhale from the ventral lung, followed by the central regions.

Discussion

On land, EIT is a useful way to assess lung disease, and to help understand lung physiology in extreme conditions. For example, Frerichs et al (2001) used it to show that lung regional ventilation and functional residual capacity change with gravity. To our knowledge, we are the first to study EIT measurement in water, both for diving humans and aquatic mammals, although underwater geophysical EIT has been used (Schuldei et al 2019, Snyder et al 2012). We are motivated by the same questions: can we better understand lung function and respiratory mechanics under the extreme physiology of diving? Can EIT be used to help evaluate lung disease in animals living in the water?

The goals of our study were to quantify and address challenges of in-water EIT, and to demonstrate the feasibility of such measurements. The key challenge is the very high conductivity of sea water – an order of magnitude larger than body tissues. Simulations demonstrate that current will flow almost exclusively in the water, and leave very little EIT

signal from the body. However, these results showed that if the water layer is kept small these problems can be addressed. We thus recommend a water layer thickness ≤ 2%, corresponding to 2 mm for an average human, which can be achieved by a relatively tight neoprene vest. For this case, signal loss is < 50% and the reconstructed image distortion is small. We next built a combined EIT belt and neoprene vest system to meet this requirement, and collected data on human volunteers and dolphins in water. Results are promising. In both cases, EIT images appear reasonable and match the expected lung physiology. In addition, the dolphin results illustrate that global EIT signals correspond closely to the spirometry-based values. Our human measurements additionally illustrate the challenges of in-water EIT. Electrode disconnection events lead to very different artefacts to their corresponding (relatively well-understood) changes in air. The use of wired EIT cables is additionally cumbersome in water, especially for unrestrained animals. Wireless devices would help, but are limited by the difficulty of transmitting signals through water.

In human divers, we want to understand the effect of training, postures, manoeuvres and fatigue on diver performance and physiology. In our human trial, the subject's tidal breathing and maximal breath holds (Figure 6), along with the novel 3D GREIT reconstruction approach, offered high-resolution imaging of lung function under uniform external pressure while submerged. The images captured distinct upper and lower lung plane activity, showing synchronized ventilation across lung regions under static conditions under water.

In dolphin trials, EIT imaging proved capable of tracking spontaneous breaths and identifying regional ventilation delays potentially linked to the dolphin's underlying pneumonia. This regional delay, absent in the healthy human data, aligns with known effects of pneumonia on airflow dynamics, possibly due to compromised tissue compliance in affected lung areas. The close alignment between EIT and pneumotachometer signals validates EIT's sensitivity to capture spontaneous breath cycles in marine mammals, though further studies with a larger sample are needed to generalize findings if EIT can be used to identify lung disease in aquatic mammals.

Our study has several limitations. FEM simulations of the conductive water were made on a cylindrical tank, rather than on body geometries, and no simulations of the effect of posture change and water movement were made. While traditional image reconstruction approaches (assuming an insulating boundary) displayed some distortions in water, we did not pursue modified image reconstructions to account for the sea water conductivity. Finally, we illustrate our results on only two subjects. Larger validation studies are underway; however, our goal here is to analyze the engineering feasibility of the technique.

This paper illustrates the feasibility of in-water EIT; however, many challenges remain. First, a tight neoprene vest is required to minimize the amount of water in contact with electrodes. This may restrict lung capacity and reduce lung compliance. The signal amplitude is strongly influenced by the water thickness t_W, meaning that movements that expel water from the neoprene will also affect measured signal levels. Movement artefacts are a big problem demonstrated in Figure 6 showing a disconnection artefact appeared during forced

exhalation, showing the sensitivity of EIT to electrode contact, especially during maximal respiratory efforts and high respiratory flow. This highlights the importance of secure electrode placement and monitoring for artefact management in submerged or dynamic conditions, which we were able to overcome mostly by our novel belt design. Experimental techniques to reduce movement are available on land; indeed, most EIT measurements have been made on supine patients with little movement. However a floating body position means subjects must make muscular movements for stability, and these movements can change posture and electrode position. Finally, electrode disconnect artefacts appear very differently. In air, electrode disconnections lead to high impedance leads, and several techniques have been developed to detect and address such events (e.g. Hartinger et al 2008). However, electrode contact impedance in water, as measured by the EIT system, will always be low. In fact, a disconnected electrode will have a lower impedance pathway to other electrodes than if it were connected. Unfortunately, this current will no longer flow through the body, and thus measurements are no longer relevant. In figure 6, electrode disconnect events are seen during larger breathing movements. We consider the management of electrode contact quality as the most important unsolved problem for EIT measurements in water. We feel a little like the fisherman in “The old man and the sea” (Hemmingway, 1952): “It is better to be lucky. But I would rather be exact."

In summary, we consider the key issue of in-water EIT – that current travels better through the water than the body. We show that EIT data quality can be ensured using a tight insulating layer, and then illustrate results in two species. EIT measurements are thus feasible in marine environments, and can be used to explore diving physiology and lung disease in diving mammals.

References

A Adler, A Fahlman, M Mosing (2024) “EIT monitoring of breathing dolphins”, p. 42, Conf. EIT 2024, Hangzhou, China.

A Adler, O Brabant, A Fahlman, A Gleiss, T Harake, M Mosing (2021) “Feasibility of Thoracic Impedance Measurements in Seawater",p.68, Conf EIT 2021, Galway, Ireland

A Adler, JH Arnold, R Bayford, A Borsic, B Brown, P Dixon, TJC Faes, I Frerichs, H Gagnon, Y Gärber, B Grychtol, G Hahn, WRB Lionheart, A Malik, RP Patterson, J Stocks, A Tizzard, N Weiler, GK Wolf (2006), “GREIT: a unified approach to 2D linear EIT reconstruction of lung images” Physiol Meas, 30:S35-S55, 2009

A Adler, WRB Lionheart (2006) “Uses and abuses of EIDORS: An extensible software base for EIT” Physiol. Meas. 27:S25-S42

Brabant O ‘EIT consensus group’, 2022. “Thoracic electrical impedance tomography – the 2022 veterinary guidelines statement”. Front. Vet. Sci. 9:946911.

KS Cheng, JC Newell, DG Gisser (1989) “Electrode Models for Electric Current Computed Tomography” IEEE T Biomed Eng 36:918–924

A Fahlman S Miedler L Marti-Bonmati, D Ferrero Fernandez, P Muñoz Caballero, J Arenarez, J Rocho-Levine, T Robeck AM Blawas (2020). “Cardiorespiratory coupling in cetaceans; a physiological strategy to improve gas exchange?", J Exp Biol 223:jeb226365

A Fahlman, MJ Moore, RS Wells (2021a) “How Do Marine Mammals Manage and Usually Avoid Gas Emboli Formation and Gas Embolic Pathology? Critical Clues From Studies of Wild Dolphins." Frontiers Marine Sci, fmars.2021.598633.

A. Fahlman, K. Aoki, G. Bale, J. Brijs, K.H. Chon, C.K. Drummond, M. Føre, X. Manteca, B.I. McDonald, J.C. McKnight, et al. (2021b). The New Era of Physio-Logging and Their Grand Challenges. *Frontiers in Physiology* **12**.10.3389/fphys.2021.669158

A Fahlman (2024). Cardiorespiratory adaptations in small cetaceans and marine mammals. Experimental Physiology 109, 324-334.

I Frerichs, T Dudykevych, J Hinz, M Bodenstein, G Hahn, G Hellige (2001) “Gravity effects on regional lung ventilation determined by functional EIT during parabolic flights” J Applied Physiol 91:39-50.

I Frerichs, M Amato, A Van Kaam, D Tingay, Z Zhao, B Grychtol, M Bodenstein, H Gagnon, S Böhm, E Teschner, O Stenqvist, T Mauri, V Torsani, C Luigi, A Schibler, G Wolf, D Gommers, S Leonhardt, A Adler (2017) “Chest electrical impedance tomography examination, data analysis, terminology, clinical use and recommendations: consensus statement of the TRanslational EIT developmeNt stuDy group”, Thorax, 72:83–93.

B Grychtol, J Schramel, F Braun, T Riedel, U Auer, M Mosing, C Braun, A Waldmann, S Böhm, A Adler (2019), “Thoracic EIT in 3D − experiences and recommendations”, Physiol Meas, 40:074006

AE Hartinger, R Guardo, A Adler, H Gagnon (2008) “Real-time management of faulty electrodes in electrical impedance tomography”, IEEE T Biomed Eng 56:369−377

Hemmingway E (1951) The old man and the sea, Bantham Books

Lemaitre F, Fahlman A, Gardette B, Kohshi K (2009) “Decompression sickness in breath-hold divers: A review" J Sports Sci 27:1519--1534.

J Schöberl (1997) “NETGEN: An advancing front 2D/3D-mesh generator based on abstract rules” Computing and Visualization in Science 1:41–52

A Schuldei, TSuthau, F John, G Ardelt, H Hellbrück (2019) ”Development of an electro impedance tomography-based platform for measurement of burial depth of cables in subsea sediments”. In OCEANS 2019-Marseille (pp. 1-8). IEEE.

Snyder, J., Silverman, Y., Bai, Y. and MacIver, M.A., 2012, October. Underwater object tracking using electrical impedance tomography. In 2012 IEEE/RSJ International Conference on Intelligent Robots and Systems (pp. 520-525). IEEE.

Z Zheng, Y Fu, K Liu, R Xiao, X Wang, H Shi (2018) “Three-stage vertical distribution of seawater conductivity” Sci Reports 8:9916